



Overlapping slabs: Untangling subduction in NW South America through finite-frequency teleseismic tomography

Meng Sun^a, Maximiliano J. Bezada^{a,*}, John Cornthwaite^b, German A. Prieto^c, Fenglin Niu^b, Alan Levander^b

^a Department of Earth & Environmental Sciences, University of Minnesota, Minneapolis, MN, USA

^b Department of Earth, Environmental and Planetary Sciences, Rice University, Houston, TX, USA

^c Department of Geosciences, Colombian National University, Bogota, Colombia

ARTICLE INFO

Article history:

Received 28 January 2021

Received in revised form 12 October 2021

Accepted 15 October 2021

Available online xxxx

Editor: H. Thybo

Keywords:

subduction
northern South America
flat slab
northern Andes
Caribbean
Nazca

ABSTRACT

Both the Caribbean and Nazca plates subduct beneath northwestern South America. The configuration of the two subducted slabs and the nature of any interaction between them has long been a matter of debate. Based on the location of intermediate-depth seismicity and active and extinct volcanism, as well as on seismic imaging, several different tectonic scenarios have been proposed. In this paper, we use teleseismic data recorded by the Colombian National Network and the temporary CARMA array in Venezuela and Colombia to produce a finite-frequency tomography model for the region. Our results show several distinct subduction segments. Through synthetic tests, we show that our results require a zone of overlap between Nazca and Caribbean subduction north of the “Caldas Tear” as has been proposed by previous studies. Additionally, we find that the Bucaramanga Nest occurs within the Caribbean Plate and coincides with bending of the slab in two planes, where both the strike and the dip of the slab change. We infer that elevated stresses are an important factor in producing the very high rates of seismicity in the nest.

© 2021 Elsevier B.V. All rights reserved.

1. Introduction

Although textbook representations of subduction zones depict a pseudo-2D geometry, where along-strike variations are ignored, real subduction zones are much more complicated. Along-strike changes in slab dip, caused by lateral variations in the structure of either the incoming or the overriding plate are not uncommon, and in some instances two different subducting slabs can be in close proximity to each other. Northwestern South America is one such complex setting. There, we find the conjunction of three plates, with the South American plate converging with both the Caribbean and Nazca plates. Matters are further complicated by the subduction of the buoyant, Cretaceous Caribbean Large Igneous Province ($\sim 1.8 \times 10^6 \text{ km}^2$) (Burke, 1988; Mora et al., 2017; Kellogg et al., 2019), and the northward migration of the Nazca plate and Nazca-Caribbean-South America triple junction in the past ~ 70 Ma (Boschman et al., 2014; Kellogg et al., 2019; Montes et al., 2019). This complex tectonic setting has spawned many conflicting hypotheses for how convergence between the different plates is

accommodated by subduction (e.g. van der Hilst and Mann, 1994; Taboada et al., 2000; Vargas and Mann, 2013; Cortés and Angelier, 2005).

Although some regional seismic tomography models exist (van der Hilst and Mann, 1994; Vargas and Mann, 2013; Chiarabba et al., 2016; Syracuse et al., 2016), resolution has been limited by station coverage. Therefore, interpretation of slab geometry in this region still relies primarily on the distribution of the intermediate-depth seismicity. Since earthquakes in this area are scarce to absent deeper than ~ 200 km, the detailed configuration of the deeper slabs is obscured. Additionally, several recent tomography studies (Chiarabba et al., 2016; Poveda et al., 2018; Syracuse et al., 2016) are based either on local seismicity or on surface wave data, leaving the deep structure beneath Colombia unconstrained. In this paper, we present a well-resolved teleseismic P-wave tomography model to investigate the configuration of subduction beneath the northern Andes. Our results reveal NE-SW trending slabs corresponding to the subduction of the Caribbean and Nazca plates, with the two subducted plates overlapping between 5°N and 8°N . Our results strongly support tectonic reconstructions that involve an overlap between the Caribbean and Nazca slabs and provide insights on the nature of some notable features in the region, namely the Caldas Tear and the Bucaramanga Nest.

* Corresponding author.

E-mail address: mbezada@umn.edu (M.J. Bezada).

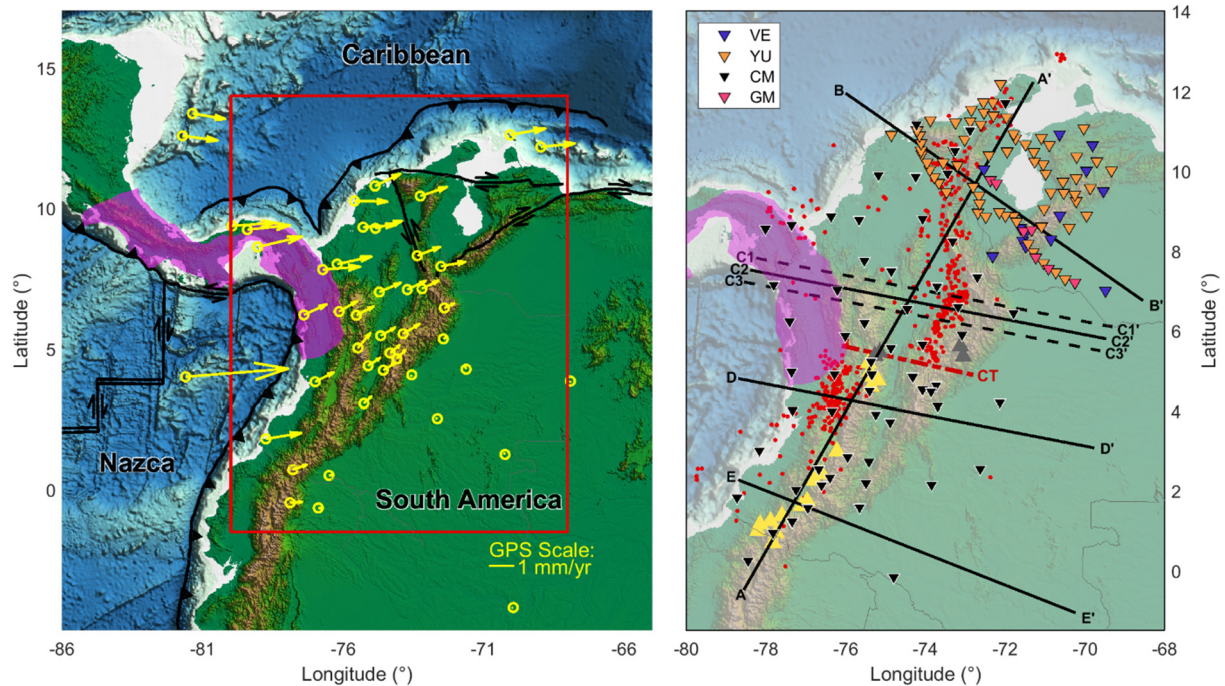


Fig. 1. Left panel: tectonic setting including GPS data from Mora-Páez et al. (2019). Red rectangle shows the location of the right panel. Right panel: Study area. Solid lines show the location of cross-sections shown in Fig. 5; dashed lines show additional cross sections shown in Fig. 6. Red dots show the location of intermediate-depth earthquakes from the Colombian Geological Service catalog. Inverted triangles show the location of seismic stations used in this study and color-coded according to the network they belong to as indicated in the legend. Seismic network abbreviations: VE – Venezuelan National Network; YU – CARMArray; CM – Colombian National Network; GM – GIAME temporary network. The purple-shaded region in each panel outlines the Panama-Choco Block. (For interpretation of the colors in the figure(s), the reader is referred to the web version of this article.)

2. Tectonic background

The Northwestern part of South America is underthrust by the Caribbean obliquely at a speed of ~ 20 mm/y while further to the east the margin transitions to a strike-slip regime (Kellogg and Vega, 1995; DeMets et al., 2000; DeMets, 2001; Weber et al., 2001; Trenkamp et al., 2002). The boundary between subducting and non-subducting Caribbean is hypothesized to form a tear in the plate, although the location and geometry of this tear are not well constrained (Bezada et al., 2010; Masy et al., 2011; Taboada et al., 2000, van Benthem et al., 2013). While intermediate-depth seismicity is relatively scarce, it has been used for decades to outline the shallow subduction of the Caribbean (e.g. Pennington, 1981; Kellogg and Bonini, 1982; Malavé and Suárez, 1995; Chiarabba et al., 2016). The subduction angle is expected to be shallow given that this region of the Caribbean is covered by the buoyant Caribbean Large Igneous Province (e.g. Burke, 1988), which possibly accounts for the absence of arc magmatism associated with this subduction. The morphology and spatial extent of the Caribbean subduction has long been a matter of debate and, although it has become clearer in the last decade, uncertainties about its lateral extent persist. Van der Hilst and Mann (1994) proposed an incipient subduction whereas Bezada et al. (2010) imaged a ~ 600 km long near-vertical velocity anomaly between 10° – 12° N implying a long-lived subduction. A slab reaching the transition zone was confirmed by van Benthem et al. (2013) and imaged in detail by Cornthwaite et al. (2021). Several authors have placed the southern edge of the Caribbean at around $\sim 10^\circ$ N (van der Hilst and Mann, 1994; Corredor, 2003; Syracuse et al., 2016), whereas others have hypothesized that it extends as far south as $\sim 5^\circ$ N (Taboada et al., 2000; Kellogg et al., 2019). Part of the difficulty in discerning the southern boundary of the Caribbean subduction is that, although the Pacific coast of Colombia is clearly part of the Nazca-South America boundary today, before colli-

sion and accretion of the Panama-Choco block (Fig. 1) it was the Caribbean that subducted beneath western Colombia (e.g. Montes et al., 2012). In fact, palinspastic reconstructions show a history of ~ 70 Ma of Caribbean subduction beneath western Colombia, starting in the Late Cretaceous and extending as far south as $\sim 2.3^\circ$ N in current coordinates (e.g. Kellogg et al., 2019; Montes et al., 2019). Northeastward motion of the Caribbean relative to South America led to the northward migration of the southern end of this boundary, and the eventual collision of the Choco Block terminated subduction diachronously from south to north (e.g. Kellogg and Mora-Páez, 2016) from 15 to 1 Ma.

Conversely, Nazca subduction below western Colombia has a diachronous onset from south to north as evidenced by the temporal evolution of volcanism (Wagner et al., 2017; Kellogg et al., 2019); which reaches as far north as 3.6° N by 20 Ma (see Fig. 7 in Kellogg et al., 2019), before eventually shutting down north of $\sim 5.5^\circ$ N at 5 Ma (Wagner et al., 2017; Kellogg et al., 2019). This leads to the present Nazca-South America plate boundary configuration in the Pacific coast of Colombia. In this modern framework, it is sensible to interpret Wadati-Benioff seismicity, volcanism and any velocity anomalies in the mantle as being related to Nazca subduction. For example, the lateral offset in intermediate-depth seismicity at $\sim 5.5^\circ$ N (Ojeda and Havskov, 2001) is most readily interpreted as a tear in the Nazca plate (the Caldas Tear, Vargas and Mann, 2013; Syracuse et al., 2016, Fig. 1). This feature coincides with the northern termination of the modern volcanic arc system in South America (Pennington, 1981; Wagner et al., 2017) and is widely thought to separate a northern flat-subducting segment of Nazca (the Bucaramanga segment) from a normally subducting (Cauca) segment to the south.

Between 5° N and 10° N, the Bucaramanga segment is thought to extend sub-horizontally to the east for 400 km before transitioning into normal subduction (Chiarabba et al., 2016; Syracuse et al., 2016). The Bucaramanga Nest, one of the world's most ac-

tive clusters of intermediate-depth seismicity (Prieto et al., 2012), appears to be located within this segment. Despite much research on the nest (e.g. Poli et al., 2016), the most fundamental questions as to which slab(s) hosts it, and whether it's of intraslab or inter-slab origin, are still debated. The nest has been variously attributed to the collision between the subducted Caribbean and Nazca slabs (van der Hilst and Mann, 1994; Zarifi et al., 2007), inflexion of the subducted Caribbean plate (Taboada et al., 2000), and a margin-parallel slab tear developed within the Caribbean plate (Cortés and Angelier, 2005; Vargas and Mann, 2013). Another dispute is about the location of the Cauca segment's northern edge. Earlier tomographic studies (Syracuse et al., 2016) and volcanic age compilations (Wagner et al., 2017) argue that the Cauca segment is limited to the north by the Caldas Tear, whereas plate reconstructions based on radiometric ages in the past 100 Ma posit there is overlap between the Cauca and Bucaramanga segments (Taboada et al., 2000; Kellogg et al., 2019).

Overall, although the existence of a gap (Caldas Tear) at a latitude of $\sim 5^\circ\text{N}$ separating the Bucaramanga and Cauca segments is evidenced by a variety of studies, e.g. seismicity and coda-Q (Vargas and Mann, 2013), Adakitic samples from Nevado del Ruiz Volcano (Borrero et al., 2009) and SKS measurements (Porritt et al., 2014). The question of whether it represents the southern edge of the Caribbean (Taboada et al., 2000; Kellogg et al., 2019) or a slab tear developed within Nazca (Vargas and Mann, 2013; Syracuse et al., 2016; Wagner et al., 2017) due to subduction of the Sandra Ridge (Lonsdale, 2005; Vargas and Mann, 2013), is still debated.

3. Data and method

Waveforms from 327 teleseismic events with good azimuthal distribution (Fig. S1) were retrieved from 151 broadband stations in the permanent Colombian National Network and the 65 stations of the CARibbean-Merida Andes temporary seismic array (CARMAr-ray) deployed from April 2016 to March 2018, along with other stations in Venezuela (Fig. 1). P arrival times from events with good signal-to-noise ratio were initially manually picked. The selected traces then underwent Gaussian bandpass filters centered at 0.3 Hz, 0.5 Hz and 1.0 Hz and, for each frequency band, relative delay times were determined by cross correlation (VanDecar and Crosson, 1990) after removing the travel time predicted by the AK135 model (Kennett et al., 1995). We then de-meaned these raw delays, obtaining 33,871 relative travel time observations.

These measurements were used as input for our velocity tomography procedure. The model is parameterized with variable node spacing to accommodate the loss of resolution with model depth as well as toward the edges of the array. Horizontal mesh node spacing is smallest inside the array footprint, where it is 42 km, and increases stepwise until it reaches 56 km 400 km outside the array. Cell height is also variable from 10 km for the shallowest layers of cells (0–60 km depth) to 60 km for the deepest layer (685–745 km depth). Eventually, the study region with a latitude range of (3.78°S, 15.96°N), longitude range of (82.75°W, 65.60°W), and depth range of (0 km, 750 km) is divided into a 40x48x24 dimensional mesh. Given their steep incidence angles, teleseismic rays cannot resolve crustal structure. To avoid mapping delay times caused by lateral variations in crustal velocity into mantle structure, we use the crustal Vs model of Poveda et al. (2018) as an *a priori* constraint. This shear wave velocity model was obtained through ambient noise tomography using 52 broadband stations in the region (Poveda et al., 2018). We estimate the corresponding absolute P wave velocities using a constant Vp/Vs ratio of 1.75. Model parameters at crustal depths (depth ≤ 40 km) are then derived by calculating the percentage variation from AK135 and imposed as a constraint on the inversion.

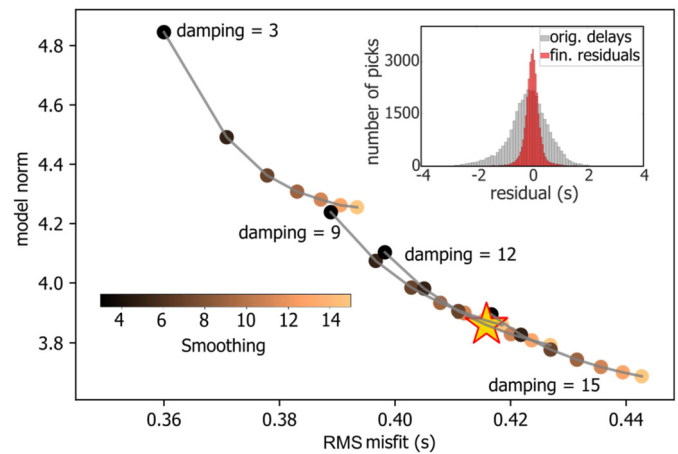


Fig. 2. L-curves used to tune hyperparameters, hyperparameter chosen in this study is denoted with a star. Inset: Histograms show the distribution of original input delays and final residuals after the inversion.

3.1. Finite-frequency tomography

The finite-frequency tomography used in our study differs from the classic ray-theoretical tomography by accounting for the effect of velocity perturbations located off the ray path and within the first Fresnel zone. This approach incorporates a better theoretical representation of wave propagation and imposes physically based smoothness criteria on the inversion; thereby reducing the reliance on *ad hoc* regularization of the inverse problem. Research comparing p-value of resulting models using ray-theoretical and finite-frequency approaches demonstrates the advantage of finite frequency theory from a statistical perspective (Larmat et al., 2017). We use an approximation to the Born theoretical sensitivity kernels commonly known as “banana doughnuts” (Dahlen et al., 2000). The sensitivity kernels are restricted to the first Fresnel zone in our study, the approximate radius of which (R_{F1}) is determined as a function of distance along the ray path (D_R) for a given frequency band (ω) and epicentral distance (Δ). Relative sensitivity within the first Fresnel zone as a function of ray-normal distance (R_N) is given by

$$K(R_N) = A \sin \left(\pi \left(\frac{R_N}{R_{F1}(D_R, \omega, \Delta)} \right)^2 \right)$$

where A is a scaling constant introduced to ensure that the integrated sensitivity through the first Fresnel zone volume is equal to that of the full Born kernel (Schmandt and Humphreys, 2010).

In addition to taking into account finite-frequency effects, we incorporate the effect of ray bending by using the hybrid ray-tracing approach of Bezada et al. (2013). This method combines 1-D ray tracing outside of the model space with a 3-D graph-theory method (Toomey et al., 1994; Hammond and Toomey, 2003) used to calculate ray locations inside the model domain. The sensitivity kernels are then constructed using the equation above where the ray-normal distance is calculated from the 3-D rays. In the first iteration, rays inside the model domain are traced through the reference 1D model to produce an initial 3D model. Subsequently, rays are traced through the model found in the previous iteration, sensitivity kernels are recalculated and the travel time residuals are inverted for updates to the model. We find that model updates become insignificant by the fifth iteration (Fig. S2). Iterations 3–5 produce nearly identical models (Fig. S3). The 5th iteration model, which we take as the preferred model, produces a variance reduction of 73.25% (Fig. 2).

3.2. Damping and smoothing regularization

The linear inversion of the time delays is an ill-posed problem. Regularization is introduced to overcome the instability of solutions and prevent overfitting. Regularization penalizes model complexity and is constructed based on the prior information of specific problems. In this study, we utilize Tikhonov regularization to penalize the norm of the model vector and add smoothness regularization.

Considering the variation of model resolution with depth, damping weights are depth-dependent. For voxels with a low hit quality, additional damping is further applied. The cost function we minimize is then:

$$J = \|Gm - d\|^2 + \lambda \|Zm\|^2 + \beta \|Lm\|^2$$

where G is the sensitivity matrix that relates the model parameters m (velocity perturbations in each voxel) to the observed delay times d , Z is a diagonal matrix that implements the depth and hit-quality dependence of damping, and L is the roughness operator. λ and β are hyperparameters defining the global weights of damping and smoothing respectively and need to be selected before inversion. We use the L-curve method to achieve the trade-off between model norm and data misfit. Values of 12 and 12 are selected as hyperparameters for damping and smoothing regularization respectively (Fig. 2). Different choices of hyperparameter values change the appearance of output model in the expected ways but the features we interpret are still present (Fig. S4). We additionally include station and event terms to absorb near-surface structure and variations in the mean travel time anomaly between different events, respectively. Model parameters that minimize the cost function are found using the LSQR method (Paige and Saunders, 1982).

3.3. Generic resolution tests

Checkerboard tests are commonly used as an indication of model resolution, although they have been shown to have important limitations (e.g. Rawlinson and Spakman, 2016). In this paper we present targeted recovery tests in section 5 that are designed to test the robustness of important features in the model. Traditional checkerboard tests are presented in the supplementary material (Figs. S5-S8) and show, as can be expected, better recovery in the north of the study area where station density is much greater. In general, anomaly amplitudes are under-recovered and the checkerboard anomalies are better recovered at depths shallower than ~ 400 km.

4. Model

In this section, we present the tomographic results by describing the geometry of velocity anomalies, paying special attention to features that are relevant to our tectonic interpretation. We image several large, continuous high-velocity anomalies (Fig. 3–6) that we interpret as distinct subducted slab segments.

Above 90 km depth, the model shows discontinuous low and high-velocity anomalies dotting the study area (Fig. 3). Given that these anomalies coincide with the locations of relatively isolated stations or station pairs (Fig. S9), this is most likely reflecting the relatively sparse station spacing in the Colombian National Network and the correspondingly spotty and discontinuous hit quality at shallow depths (Fig. 7). Alternatively, or additionally, these anomalies may be caused by errors in the assumed crustal model. Between 90 and 200 km, anomalies coalesce to delineate what we view as five distinct high-velocity bodies trending roughly NNE-SSW, parallel to the strike of the margin, which we interpret as

subducted lithosphere (Fig. 3–6). Four of the imaged slab segments are well-aligned with subduction-related volcanism and/or Wadati-Benioff seismicity (Fig. 3, 4). For convenience, in the following we refer to these four segments, from north to south, as the Maracaibo, Bucaramanga, Cartago and Pasto segments (Fig. 4). We note that previous authors refer to the slab south of 5.5°N as the Cauca segment. Here, because we see differing characteristics in the velocity anomalies, the abundance of intermediate-depth seismicity and volcanism, we divide that segment into Cartago and Pasto north and south of $\sim 3^\circ\text{N}$ respectively.

The Maracaibo segment spans the length of the Caribbean coast of Colombia and has a convex-west geometry along strike that follows the curvature of the trench. A vertical cross-section through the model shows a subducted slab with a dipping angle of $\sim 45^\circ$ above ~ 350 km and $\sim 60^\circ$ below ~ 350 km (Fig. 5, cross section BB').

Further south, the Bucaramanga segment underthrusts South America with a strike of $\sim \text{N}10^\circ\text{E}$, and an abrupt change in dip angle at a depth of ~ 150 km (Fig. 5, cross section CC'). At that depth, the Bucaramanga segment also exhibits a change in slab strike from $\sim \text{N}10^\circ\text{E}$ north of 7°N to $\sim \text{N}35^\circ\text{E}$ further south (Fig. 3, 4). This change in slab strike and dip spatially coincides with the Bucaramanga Nest. West of the Bucaramanga segment, between 5° and 8°N , additional high velocity anomalies are imaged with amplitudes of $\sim 2\text{--}3\%$ (compared to $\sim 4\%$ in the Bucaramanga segment). These anomalies are less continuous and trend roughly NE-SW. They are most clear at 90–230 km depth, but spatially smaller anomalies are found all the way down to the transition zone (Fig. 3). We tentatively interpret this as an additional, distinct, slab segment (Medellín segment, Fig. 4) and will test whether these anomalies can instead be produced by shallowly subducting lithosphere belonging to the Bucaramanga segment in the following section.

The southern end of the Bucaramanga segment coincides with the lateral shift in intermediate-depth seismicity that has been dubbed the Caldas Tear at 5.5°N (Vargas and Mann, 2013). South of there, we image the third clear slab segment (Cartago) that is co-located with intermediate-depth seismicity and thus ~ 250 km west of the Bucaramanga segment to the north. The offset between these two slab segments appears to decrease with depth, with the tear seeming to close by ~ 200 km (Fig. 3). At a latitude of $\sim 3^\circ\text{N}$, we find another gap separating the Cartago and Pasto segments. Synthetic tests suggest this gap is real (see section 5), although resolution in this part of the model is relatively poor. The imaged gap coincides with an along-strike change in the density of intermediate-depth seismicity as well as the spatial frequency of volcanoes (Fig. 4, Fig. S10) so we interpret it as marking the boundary between two distinct slab segments with different physical characteristics. Below 230 km, the magnitude of the Pasto segment anomaly fades to zero.

An intriguing observation is that although above 270 km the Maracaibo, Bucaramanga and Cartago segments show distinct characteristics (including strike, dip and seismic productivity), they appear to merge into a single feature by 270 km depth and form a remarkably continuous linear slab by 400 km depth (Fig. 3). This continuous slab-like feature is consistently observed down to the bottom of the transition zone where it seems to lay flat over the 660 km discontinuity.

5. Testing possible slab configurations

In interpreting our tomography model we are mindful that, like all seismic models, it is an imperfect representation of the subsurface. The true slab structure is to some degree distorted by the imperfect station coverage and ray distribution, in addition to the inherent limitations of travel-time tomography. In this section, we

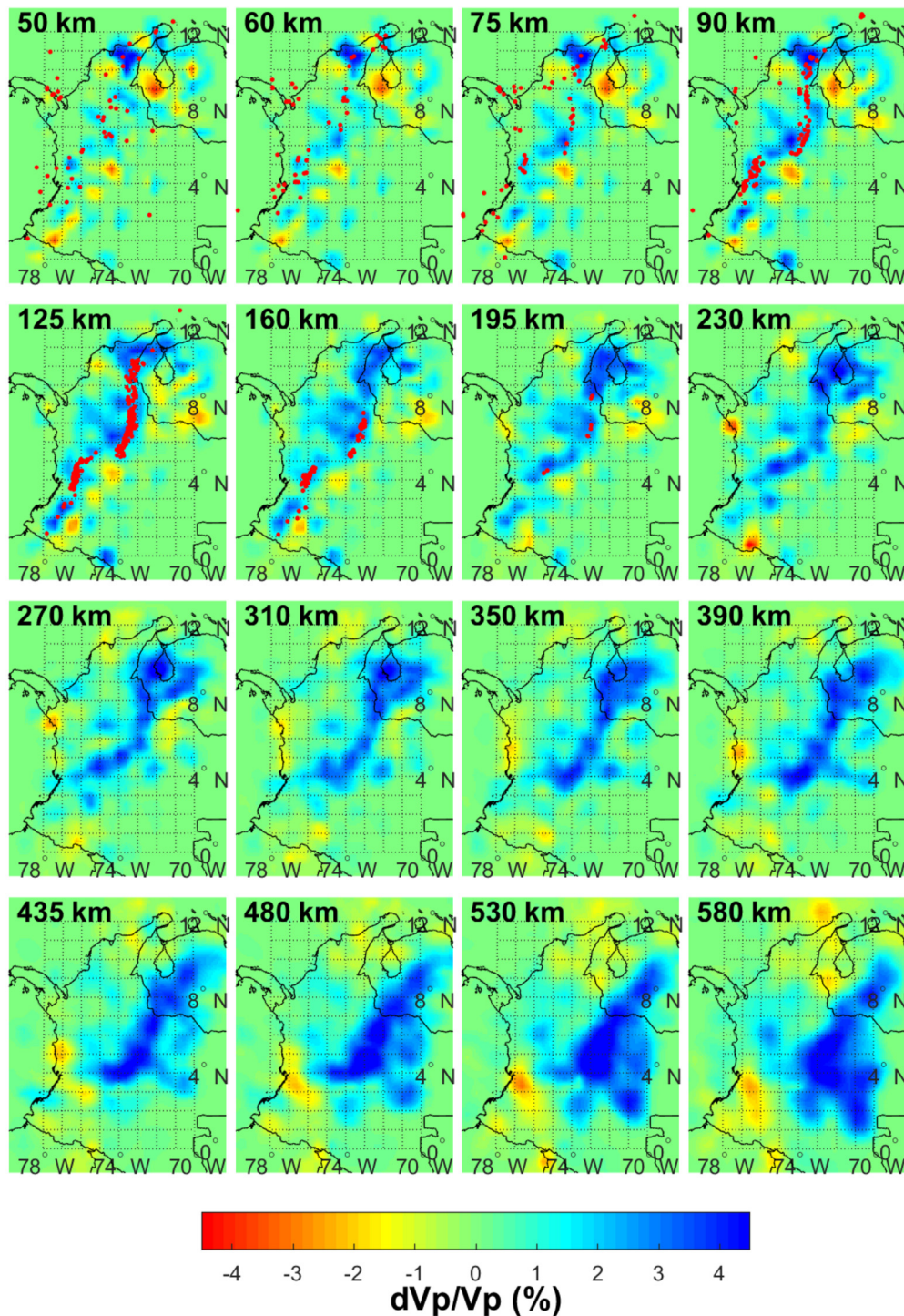


Fig. 3. Tomography results, map view at different depths as indicated in each panel. Seismicity is denoted as red circles at corresponding depths.

investigate how various subduction configurations would be represented by our tomography procedure to inform our interpretation. We seek to answer the following questions:

- 1) Do the anomalies we have tentatively labeled as Medellín segment represent subducted lithosphere, or are they likely to be streaking artifacts (incorrect mapping to depth of shallower velocity anomalies)?
- 2) Do the Bucaramanga and Cartago segments truly merge at depth, or is there a different explanation for the imaged geometry?

- 3) Are the gaps we image between slab segments real or are they an artifact of incomplete station coverage?

Questions 1 and 2 above are especially important for a tectonic interpretation. The fact that the Maracaibo, Bucaramanga and Cartago segments appear to merge into a single, continuous feature suggests a common origin for this lithosphere. This would mean they are all fragments of either the Caribbean or Nazca plates. A common Nazca origin can be ruled out because we can follow the Maracaibo segment unequivocally to the Caribbean coast as far north as $\sim 11^\circ\text{N}$ and Nazca subduction has never reached

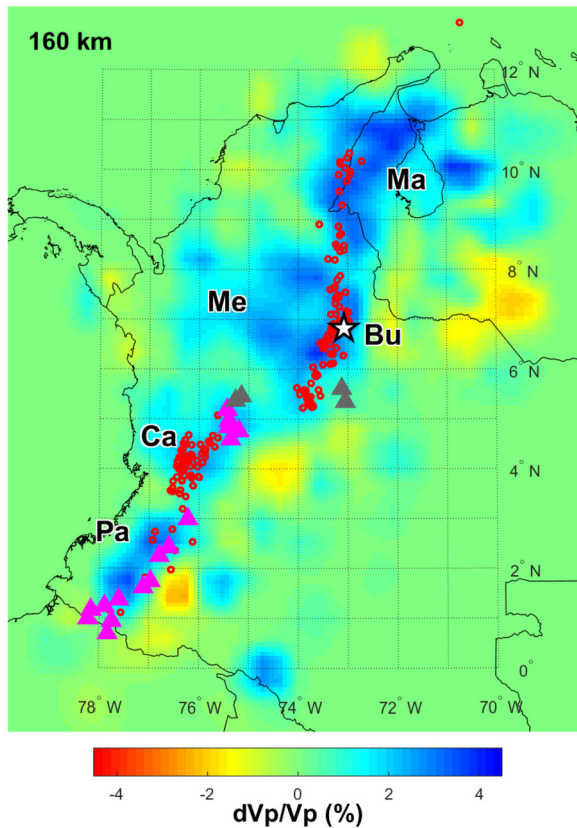


Fig. 4. Tomography result, slice at 160 km depth with the names of the different segments we refer to in the text. Seismicity between 120 and 180 km depth is denoted as red circles. Solid and open triangles represent active and inactive volcanoes, respectively. The white star marks the location of the Bucaramanga Nest. Segment name abbreviations: Ma – Maracaibo; Bu – Bucaramanga; Me – Medellín; Ca – Cartago; Pa – Pasto.

that latitude. The Maracaibo segment must be Caribbean. On the other hand, a common Caribbean origin for all three segments can also be ruled out because the Cartago segment is clearly related to active volcanism that can only be a product of Nazca subduction (Taboada et al., 2000; Wagner et al., 2017; Mora et al., 2017; Kellogg et al., 2019). The Cartago segment must belong to Nazca. Meanwhile, the continuity in intermediate-depth seismicity and velocity anomalies between the Maracaibo and Bucaramanga segments strongly suggests a common, Caribbean, origin. Yet, young volcanism occurring as far north as $\sim 8^\circ\text{N}$ (north of the southern end of the Bucaramanga segment) can only be attributed to Nazca subduction, given that it occurs well after the collision and accretion of the Panama-Choco block (Wagner et al., 2017; Mora-Paez et al., 2019; Kellogg et al., 2019). These apparently conflicting lines of evidence can be resolved if there is overlapping Nazca and Caribbean subducted slabs between $\sim 5.5^\circ\text{N}$ and $\sim 7^\circ\text{N}$ as has been suggested by Kellogg et al. (2019) and others. In this scenario, the Pasto, Cartago and Medellín segments would all be subducted Nazca lithosphere while the apparent merging of the Cartago and Bucaramanga segments is explained by a change in along-strike width of the Bucaramanga segment, with the southern end moving further south with depth.

5.1. Synthetic input models

To test the different hypotheses outlined above we design three variations of a synthetic model containing slabs representing Caribbean and Nazca subduction. We note that the goal of these tests is not to exactly replicate what is recovered in the

inversion of real data, as the detailed geometry is difficult to reproduce, but rather to investigate the questions posed at the beginning of this section. The synthetic models include different slab segments, all with anomaly amplitudes of 5%. Between $5^\circ\sim 12^\circ\text{N}$, we assume a continuous slab in the depth range of $50\sim 660\text{ km}$, with its southern edge expanding southwards in depth to $\sim 4^\circ\text{N}$. This segment is common to all three variations and represents a Caribbean slab that includes the Maracaibo and Bucaramanga segments. The slab geometry includes a change in dip from 20° to 70° at a depth of $\sim 120\text{ km}$ to emulate the observations of the Bucaramanga segment. At $90\text{--}150\text{ km}$ depth the synthetic slab coincides with intermediate-depth seismicity, although we don't include the change in the trend of the seismicity at the Bucaramanga Nest (Fig. 4). Other slab segments represent the Nazca subduction and their geometry is different in each variation:

Variation I: A continuous slab extending between $50\sim 300\text{ km}$ along depth and $0^\circ\text{--}5^\circ\text{N}$ along latitude, following the trend of the intermediate-depth seismicity (Fig. 8, left column). In this variation there is no overlap with the Bucaramanga segment. The hypothetical Nazca slab reaches a depth of 650 km .

Variation II: Similar to above but extending from 0° to 8°N , overlapping with the Bucaramanga segment between $5^\circ\text{--}8^\circ\text{N}$ (Fig. 8, middle column). This would represent a continuous slab including the Pasto and Cartago segments, along with the Medellín segment. In this case, the hypothetical Nazca slab only reaches a depth of 350 km .

Variation III: As in II, the slab extends to 8°N along latitude, but with a gap between $5.5^\circ\text{--}6.5^\circ\text{N}$ (Fig. 8, right column). In this configuration there is overlap with the Bucaramanga segment between $6.5^\circ\text{--}8^\circ\text{N}$ and a clear separation between the Cartago and Medellín segments.

For each of these variations of the input model, synthetic delay times were calculated using the same event-receiver geometry as for the real data. We then invert the synthetic data sets with the same procedure, regularization, and number of iterations as with the real data. Comparison of the known input and inverted output models helps distinguish robust features from imaging artifacts.

5.2. Synthetic results

Firstly, as shown in Fig. 8 and Fig. 9, a comparison of the synthetic input and output models demonstrates that our source-receiver geometry is able to accurately resolve the target structures deeper than $\sim 200\text{ km}$; as the locations and characteristics of the input velocity anomalies are well recovered by the inversion. We focus this discussion on aspects of the synthetic test results that have a direct bearing on the tectonic interpretation of the inversion of real data. Inspection of the recovered synthetic structures leads to the following conclusions:

A) As can be expected, subhorizontal subduction is not imaged as a high-velocity anomaly. Comparison between the input and output of synthetic model I (Fig. 8 vs. Fig. 9) implies weak resolution for subhorizontal slabs at shallow depths as may be found in the Maracaibo and Bucaramanga regions. The difficulty in imaging shallow, areally large sub-horizontal anomalies is a well-known limitation of teleseismic tomography. Other studies have similarly shown poor recovery of synthetic flat slabs, even with much denser station coverage (e.g. Scire et al., 2016). Importantly, this implies that the high-velocity anomalies to the west of the Bucaramanga segment in the inversion of real data (Medellín segment) are not a product of streaking of high-velocity anomalies related to a flat slab.

B) High velocity anomalies west of the Bucaramanga slab require the presence of the subducted Nazca lithosphere north of 5.5°N . The secondary feature behind the Bucaramanga segment (Medellín segment, Fig. 4, Fig. 6) is only successfully reproduced

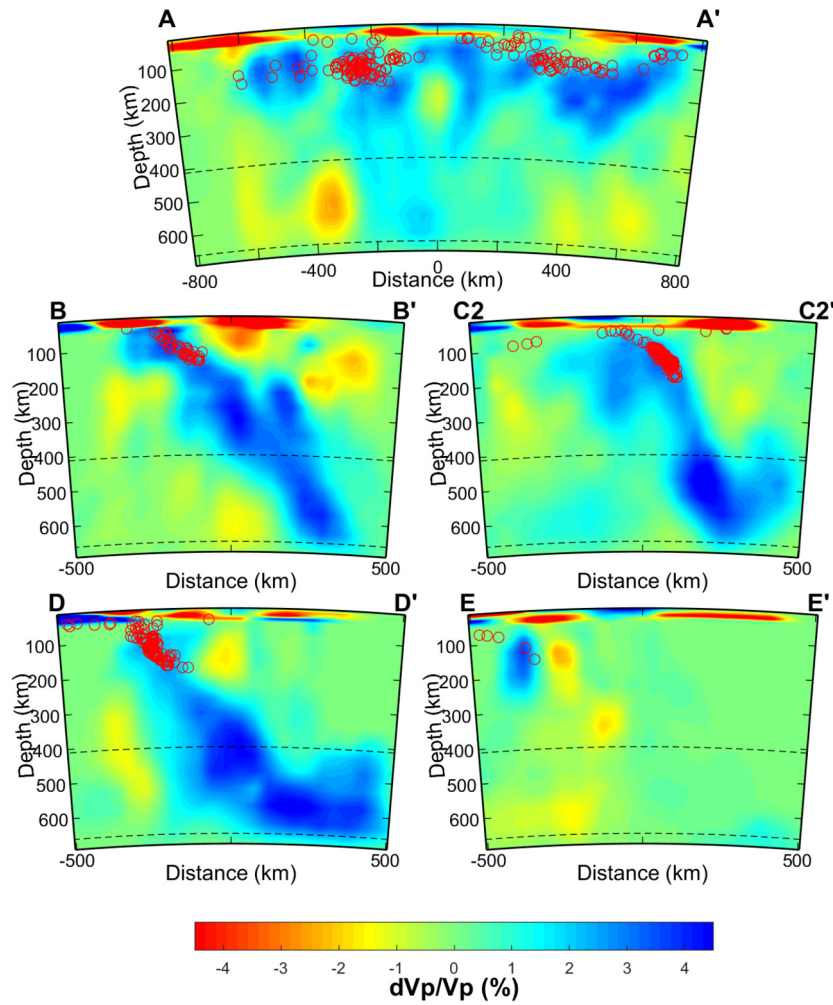


Fig. 5. Tomographic cross sections along lines AA'-EE' in Fig. 1. Note the A and A' points correspond to the SSW and NNE ends of the line, respectively. Red open circles show seismicity within 50 km of the profile.

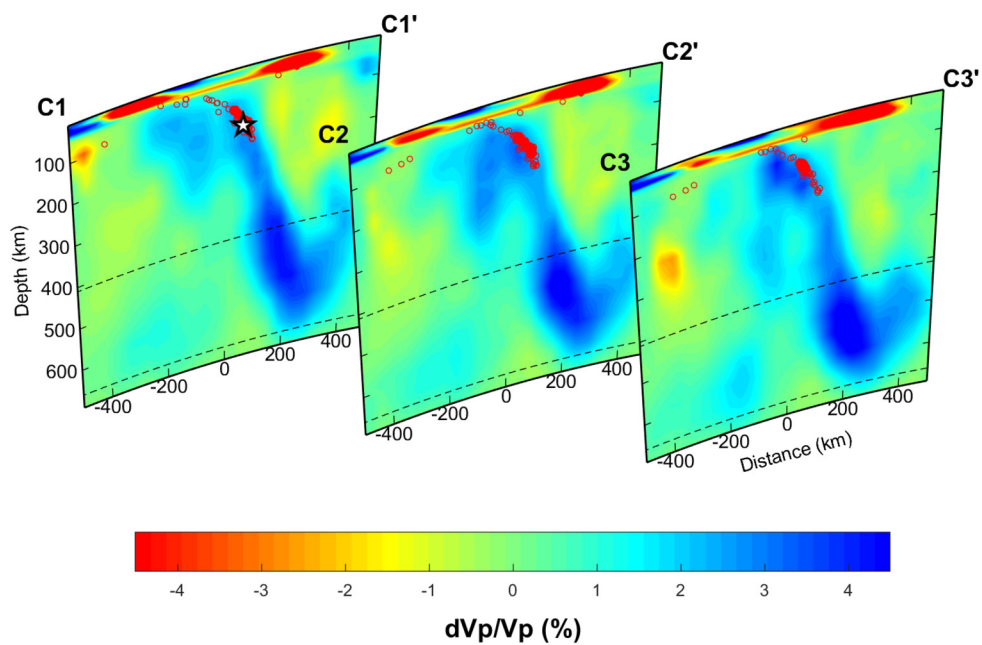


Fig. 6. Tomographic cross-sections showing secondary features to the west of the Bucaramanga segment (main slab in the profiles) along profiles C1-C1', C2-C2', C3-C3'. See Fig. 1 for the location of the profiles. Red circles show seismicity within 50 km of the profile. The white star on profile C1-C1' marks the location of the Bucaramanga Nest.

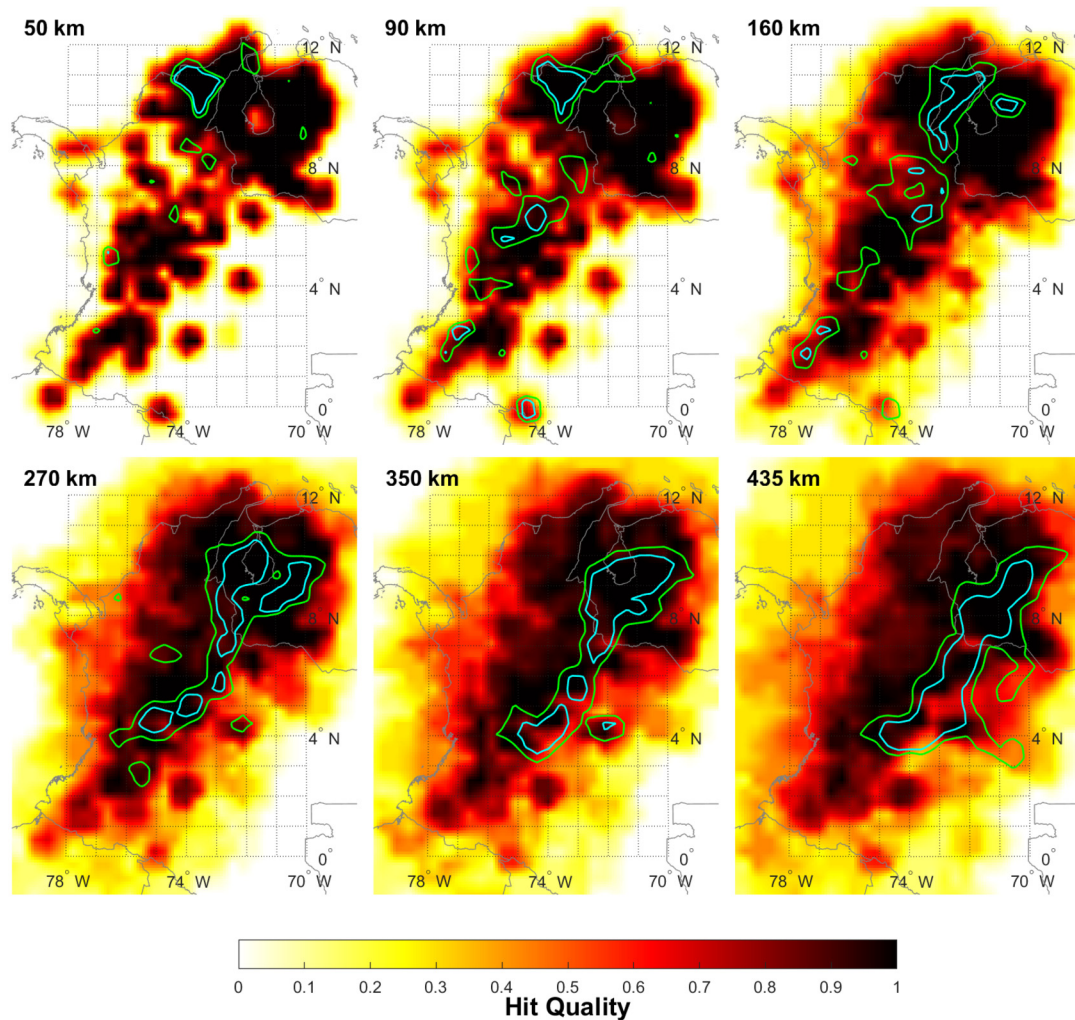


Fig. 7. Hit quality, with slab contours with 2%, and 3% anomaly contours shown by green and cyan lines respectively. Hit quality is defined as in Schmandt and Humphreys (2010) by taking into account the number of rays in each backazimuth quadrant.

(Fig. 9) when additional anomalies representing a northward extension of the Nazca slab (overlapping the Caribbean Bucaramanga segment) are introduced in the synthetic input (Fig. 8); while no artificial features are generated if there is no overlap (Fig. 8, Fig. 9). The short, near-vertically dipping anomaly attached to the surface in Fig. 9 (profile C2-C2') is consistently recovered along strike where Nazca and Caribbean overlap. This recovered synthetic geometry is most similar to that found along the same profile in the model derived from real data (Fig. 5, 6, 9).

C) Along-strike gaps separating the imaged slab segments are likely real features. The gap observed between the Cartago and Medellín segments between 5.5°N and 6.5°N in Fig. 4 is only reproduced when a gap exists between the synthetic slabs (Fig. 8, 9 top row), which indicates there likely is a gap at this location, rather than an improperly recovered continuous slab. Further south, at $\sim 3^{\circ}\text{N}$ the real model shows a gap between what we have called the Cartago and Pasto segments. In contrast, synthetic outputs successfully recover the prescribed continuous slab in this area, with no gap artificially generated at $\sim 3^{\circ}\text{N}$ (Fig. 8, 9). This suggests that the gap between these two slab segments is also a real feature.

D) There may be flat-lying Caribbean slab material atop the 660 km discontinuity. Tomography results in section 3 show flat-lying slab material at depths of 500–660 km (Fig. 3, 5). In the synthetic test, the input models have no flat-lying velocity anomalies at these depths. Accordingly, in the corresponding output velocity

models, there are no artificially generated sub-horizontal anomalies at the bottom of the transition zone. This result suggests that the deep anomalies east of the toe of the slab in the model derived from real data are robust. However, given the limited resolution at this depth, and the fact that the model domain does not extend to the lower mantle, this study is not well-suited to constrain the deeper slab geometry and we do not discuss the issue further.

6. Discussion

Resolving the debate about the current configuration of subduction beneath the northern Andes has been hindered by the lack of constraints in the deeper subsurface structure. Here, taking advantage of the Colombian National Network and a dense temporary deployment, we provide a well-resolved tomography velocity model of Colombia and western Venezuela.

Considering the results of the tests described in section 5, our tomography model is most consistent with the scenario described by Kellogg et al. (2019), and hypothesized by others (e.g. Cortés and Angelier, 2005; Taboada et al., 2000). Namely, there is about 200 km of overlap between the Caribbean and Nazca subductions between $\sim 5.5^{\circ}$ and $\sim 7.5^{\circ}\text{N}$. The subducted Caribbean slab extends from $\sim 11^{\circ}\text{N}$ to $\sim 5.5^{\circ}\text{N}$ at ~ 100 km depth, with its southern end extending further south with increasing depth to $\sim 3^{\circ}\text{N}$ below 300 km, and includes the Bucaramanga and Maracaibo segments. The offset of intermediate-depth seismicity at the “Caldas

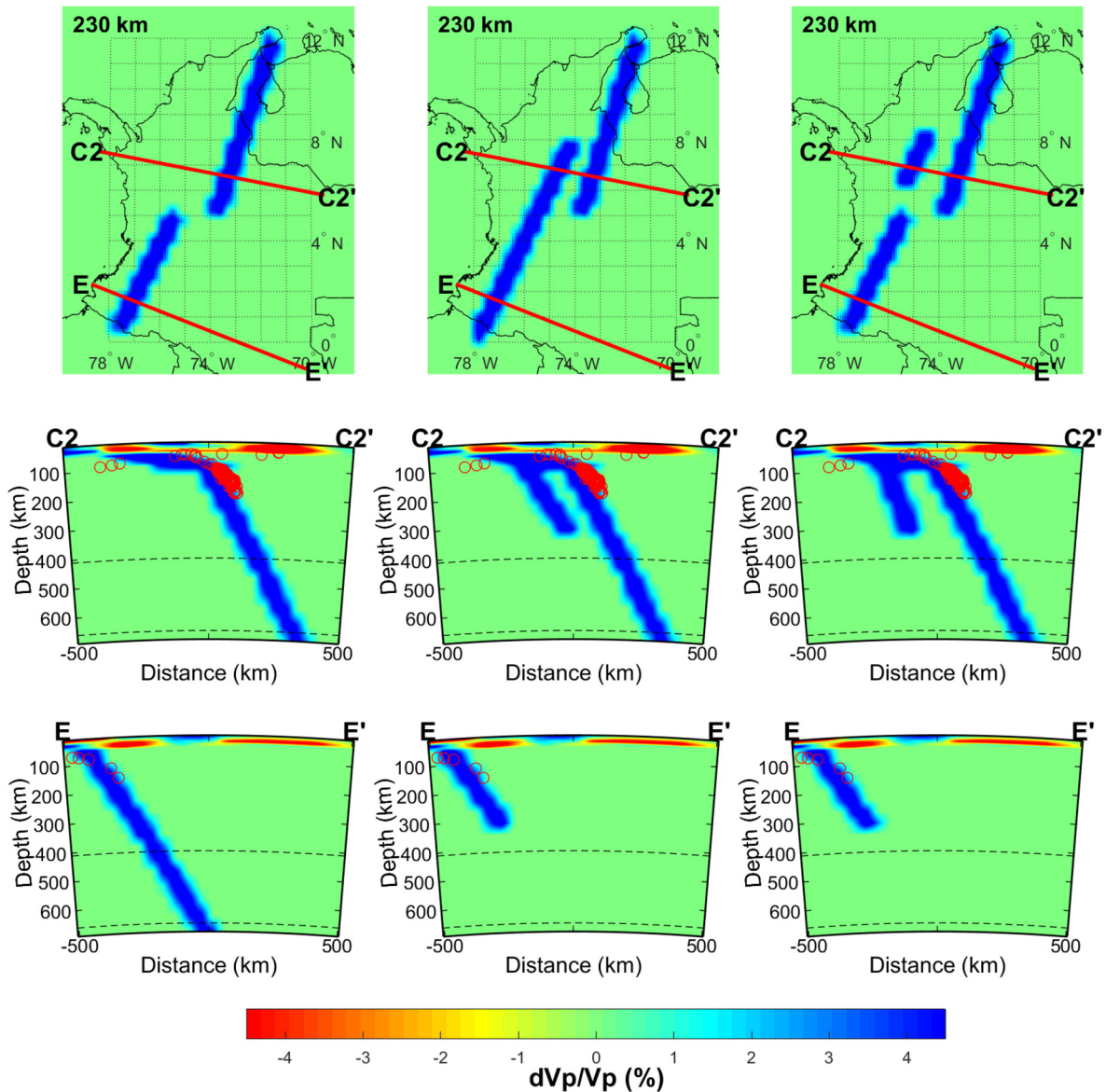


Fig. 8. Three synthetic input models. First row: Map view at 230 km depth with locations of profiles indicated by red lines, see also Fig. 1. Second row: Cross-sections along profile C2-C2'. Third row: Cross-sections along profile E-E'. The three columns, from left to right, show synthetic model variations I, II and III described in the text.

Tear”, marks the southern end of Caribbean subduction instead of offset between two Nazca segments, in accordance with Kellogg et al. (2019). Nazca subduction does seem to be fragmented in our study area, with three distinct segments, from north to south: The Medellín segment north of the “Caldas Tear” is the one that overlaps with Caribbean subduction and shows no volcanism or intermediate-depth seismicity (Fig. 3, 4). The Cartago segment, directly south of the “Caldas Tear” and north of $\sim 3^{\circ}\text{N}$ shows relatively abundant intermediate-depth seismicity and is co-located with active volcanism (Fig. 3, 4). Finally, the Pasto segment south of 3°N is related to volcanism in the surface and shows a modest amount of intermediate-depth seismicity (Fig. 3, 4). The southern end of the Pasto segment lies outside our study area, but inspection of the intermediate-depth seismicity hypocenters suggests its southern terminus is $\sim 1.3^{\circ}\text{S}$, given that south of that latitude the density of intermediate-depth seismicity increases again (Fig. S10).

The Bucaramanga slab segment has been variably attributed over the decades to Caribbean (Taboada et al., 2000; Cortés and Angelier, 2005; Kellogg et al., 2019) or Nazca (Syracuse et al., 2016; Wagner et al., 2017) lithosphere. Hypotheses arguing

for a Caribbean origin are mainly based on the continuous distribution of intermediate-depth seismicity from $\sim 11^{\circ}\text{N}$ to 5.5°N , across the Bucaramanga and Maracaibo segments, at a depth range of 90–150 km (e.g. Kellogg et al., 2019. Fig. 1, 3, 4); as well as by palinspastic reconstructions (e.g. Kellogg et al., 2019; Montes et al., 2012, 2019; Cortés and Angelier, 2005). In contrast, a Nazca origin is suggested not only by the current position and direction of the Nazca plate with respect to South America, but also from compilations of volcanic ages in the past 14 Ma (Wagner et al., 2017). Wagner et al. (2017) point out that arc volcanism associated with Nazca subduction extended along Colombia’s entire Pacific margin in the mid-Miocene. They interpret a shut-off of volcanic activity north of $\sim 3^{\circ}\text{N}$ at ~ 6 Ma as the onset of flat-slab Nazca subduction, with arc volcanism resuming only south of 5.5°N after 4 Ma. This pattern was interpreted by Wagner et al. (2017) as showing Nazca slab flattening at 6 Ma and subsequent tearing at the Caldas Tear, resulting in a flat slab segment to the north (Bucaramanga) and a re-steepened segment to the south (Cauca, which we separate into Cartago and Pasto).

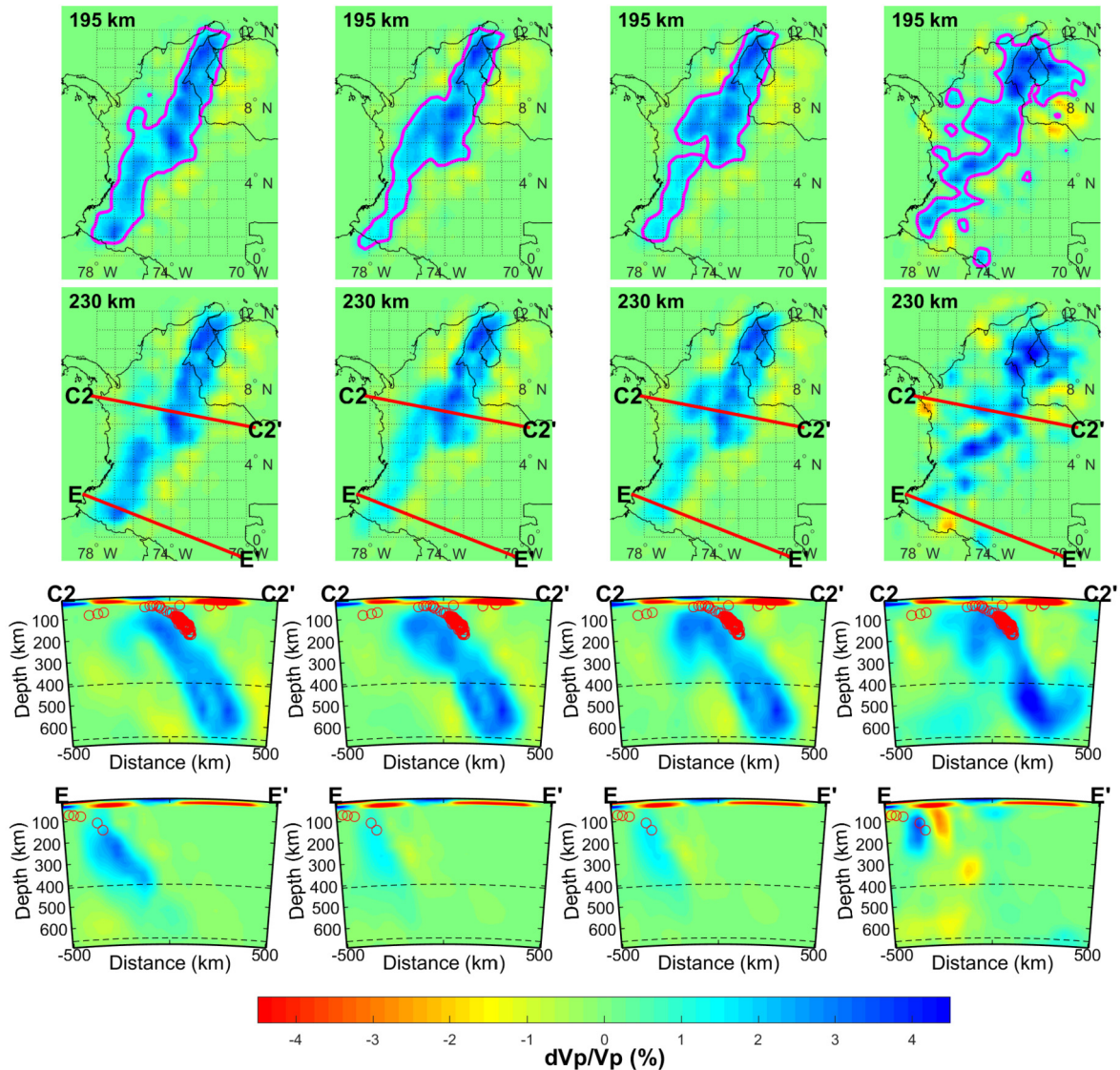


Fig. 9. Inversion results of synthetic models variations I-III (first three columns) and the real data (fourth column) for comparison. First row: Map view at 195 km depth; the 1% contour is indicated in magenta to highlight slab continuity or gaps in the slabs. Second row: Map view at 230 km and profile locations. Third row: Cross-sections along profile C2-C2'. Third row: Cross-sections along profile E-E'.

Our tomography results show a laterally continuous slab-shaped positive velocity anomaly spanning all the northern Andes (3°N - 10.5°N) at depths deeper than 300 km (Fig. 3). This is strong evidence supporting a common origin for the Maracaibo and Bucaramanga segments, that can only be associated with the Caribbean as discussed in section 5. Distinct morphologies of these two segments at shallower depths (90-300 km), including different strike and dip (Fig. 3, 4), are likely an expression of the heterogeneity in crustal and lithospheric structure of the incoming Caribbean plate along strike and the diachronous collision of the Panama-Choco block at the trailing end of the plate (e.g. Kellogg et al., 2019; Montes et al., 2019). Furthermore, the spatial extent of the subducted Caribbean slab as constrained by our tomographic results is highly consistent with estimates of the length of the trench in the geologic past as presented in several recent palinspastic reconstructions (e.g. Kellogg et al., 2019; Montes et al., 2019). We interpret this slab to be attached to the Panama-Choco block which sutured to South America in the Middle Miocene (e.g. Montes et al., 2019). Terrane accretion is commonly thought to be followed by slab breakoff and detachment (Davies and von Blanckenburg, 1995; Garzanti et al., 2018 and references therein), yet

“fossil” slab fragments in some cases remain attached for tens of Ma (e.g. Schmandt and Humphreys, 2011). Our results suggest that the subducted Caribbean lithosphere connected to the Panama-Choco block has not yet detached.

Additional high-velocity anomalies are observed to the west of the Bucaramanga segment between $5^{\circ}\sim 8^{\circ}\text{N}$ and synthetic tests rule out the possibility that these are merely imaging artifacts. Instead, we interpret these anomalies as the northernmost expression of Nazca subduction (Medellín segment), where it subducts beneath the Choco block, once a part of the Caribbean but currently accreted to South America (Kellogg et al., 2019; Montes et al., 2019). This interpretation is consistent with plate reconstruction studies (Kellogg et al., 2019; Montes et al., 2019) that argue for exactly this sort of overlap between Nazca and the Caribbean based on the dating of volcanism and deformation in the past ~ 100 Ma, as well as with current GPS observations (Kellogg and Vega, 1995; DeMets et al., 2000; DeMets, 2001; Weber et al., 2001; Trenkamp et al., 2002).

The imaged slab geometry is consistent with the volcanic history described by Wagner et al. (2017). As Kellogg et al. (2019) point out, the spike in volcanic activity in the Choco terrane and

just east of the terrane from 15 to 5 Ma was indeed related to Nazca subduction, but the overriding plate was the Caribbean. In their interpretation, the abrupt cessation of volcanic activity to the north of 5.5°N ~6 Ma can be explained by thermal isolation caused by the Nazca slab coming up to the subducted Caribbean slab. An outstanding question is why volcanism ceased as far south as ~3°N if the southern limit of slab overlap (and the hypothesized thermal isolation) is 5.5°N. We propose as a working hypothesis that as the Nazca trench approached the Caribbean slab, mantle wedge suction (e.g. Ma and Clayton, 2015) may have indeed produced some flattening of the northern end of Nazca, as far south as ~3°N, where we place the limit between the Cartago and Pasto segments. Subsequently, the Cartago segment (3°–5.5°N) would have resteepped and resumed volcanism, while the Medellín segment remained avolcanic given its overlap with Caribbean lithosphere as described by Kellogg et al. (2019). This scenario would provide a mechanism for slab flattening of northernmost Nazca, which remained unidentified in Wagner et al. (2017). Under this hypothesis, there would indeed be a tear in the Nazca plate at 5.5°N but it would be different in nature from what was originally posited as the Caldas Tear by Vargas and Mann (2013).

One important argument against our interpretation is the lack of intermediate-depth seismicity associated with the Medellín segment. The different slab segments we image vary in the density of their seismicity, with intermediate-depth earthquakes being much sparser in the Pasto segment than in the Cartago segment, for example (Fig. 4, S10). However, the Medellín segment is the only one for which intermediate-depth seismicity is completely absent. While puzzling, this observation is not unprecedented. The subduction of the Juan de Fuca plate (another remnant of Farallon, e.g. Atwater, 1970) is bracketed to the north and south by the subduction of the Explorer and Gorda microplates, respectively (e.g. Stock and Lee, 1994). Neither of these microplates show seismicity below ~60 km (e.g. McCrory et al., 2012), in spite of appearing as high-velocity anomalies at those depths in tomography models (e.g. Bodmer et al., 2018). Although we have referred to the Cartago and Medellín segments as Nazca subduction (in accordance with most authors), in northernmost Nazca two microplates have been identified: the Malpelo and Coiba microplates (e.g. Adamek et al., 1988; Zhang et al., 2017). What we have defined as the Medellín segment may be more accurately described as subducted Coiba lithosphere. Coiba lithosphere is young (<10 Ma, e.g. Müller et al., 2008) and may be too warm to host intermediate-depth seismicity. This scenario would be somewhat analogous to Gorda or Explorer subduction, with the added complication of the overlap with the Caribbean slab. We note that the amplitude of the high-velocity anomaly we interpret as the Medellín segment is generally smaller than that of the Bucaramanga segment (Fig. 6) consistent with Medellín being a relatively warm slab.

Lastly, our interpretation has implications for the origin of the Bucaramanga Nest. This volume of intense intermediate-depth seismicity has been interpreted as occurring within the Nazca plate (e.g. Chiarabba et al., 2016), within the Caribbean plate (Taboada et al., 2000; Cortés and Angelier, 2005; Prieto et al., 2012), and at the boundary of the two (van der Hilst and Mann, 1994; Zarifi et al., 2007; Syracuse et al., 2016). The unusually high concentration of seismicity has been attributed to the tip of a propagating slab tear (e.g. Vargas and Mann, 2013; Cortés and Angelier, 2005), and to the subduction of extraordinarily hydrated lithosphere (e.g. Chiarabba et al., 2016). According to our interpretation of the tomography model presented here, the Bucaramanga Nest is located in the interior of the subducted Caribbean plate. Furthermore, the nest coincides with elevated curvature in the slab surface; it is located where there is both a large increase in dip and a change in the strike of the slab (Fig. 3, 4, 6). Modeling has shown that slab bending and the associated larger strain rates produce zones

of elevated stress within subducted slabs (Billen, 2020). Although we cannot rule out a contribution by locally enhanced hydration of the slab, we suggest that elevated stresses related to the high curvature of the slab in both a vertical and horizontal plane play an important role in the concentration of seismicity at the Bucaramanga Nest. The likely complicated stress distribution at a doubly bending point in the slab may help explain the diversity of focal mechanisms found in the Bucaramanga Nest (e.g. Prieto et al., 2012; Poli et al., 2016).

7. Conclusions

In this paper, we provide a well resolved P wave velocity model of the NW South America subduction zones. Some features proposed by previous work are further confirmed and several new features with significant implications are observed for the first time. To summarize:

- The Maracaibo and Bucaramanga segments are of Caribbean origin, with the Caldas Tear being the southern edge of the subducted Caribbean plate. The southern edge of this slab propagates southward with depth. Differences at shallow depths between these two segments are likely an expression of heterogeneity in the incoming Caribbean plate and the diachronous collision of the Panama-Choco block.
- The Bucaramanga Nest is hosted within the subducted Caribbean plate where there is an abrupt change in both dip and strike at depths of ~150 km. The enhanced stress produced by bending on two planes may be the primary cause of the high seismicity rate rather than excess dehydration; although some contribution from this mechanism can't be ruled out by our images.
- The Nazca plate is observed to overlap with Caribbean plate between 5.5°~8°N, by what we are calling the Medellín segment. South of ~5.5°N (latitude of the Caldas Tear), we identify the Cartago and Pasto segments (Cauca segment for previous authors). The three slab segments that we interpret as having a Nazca origin differ in the amount of volcanism and intermediate-depth seismicity associated with them.

CRediT authorship contribution statement

Meng Sun: Formal analysis, Visualization, Writing – original draft. **Maximiliano J. Bezada:** Conceptualization, Methodology, Supervision, Visualization, Writing – review & editing. **John Cornthwaite:** Formal analysis, Writing – review & editing. **German A. Prieto:** Conceptualization, Writing – review & editing. **Fenglin Niu:** Conceptualization, Writing – review & editing. **Alan Levander:** Conceptualization, Writing – review & editing.

Declaration of competing interest

The authors declare that they have no known competing financial interests or personal relationships that could have appeared to influence the work reported in this paper.

Acknowledgements

We thank the Colombian Geological Service and the Venezuelan Foundation for Seismological research for providing data from their permanent and temporary stations and for their operation of the CARMA seismic array. The US seismic instruments were provided by the Incorporated Research Institutions for Seismology (IRIS) through the PASSCAL Instrument Center. The facilities of the IRIS Consortium are supported by the National Science Foundation's Seismological Facilities for the Advancement of Geoscience (SAGE)

Award under Cooperative Support Agreement EAR-1851048. This research was partly supported by the National Science Foundation under Grant No. EAR-1459047. We thank two anonymous reviewers who provided valuable feedback that helped improve the manuscript.

Appendix A. Supplementary material

Supplementary material related to this article can be found online at <https://doi.org/10.1016/j.epsl.2021.117253>.

References

- Adamek, S., Frohlich, C., Pennington, W.D., 1988. Seismicity of the Caribbean-Nazca Boundary: constraints on microplate tectonics of the Panama region. *J. Geophys. Res., Solid Earth* 93 (B3), 2053–2075. <https://doi.org/10.1029/JB093iB03p02053>.
- Atwater, Tanya, 1970. Implications of plate tectonics for the Cenozoic tectonic evolution of western North America. *Geol. Soc. Am. Bull.* 81 (12), 3513–3536.
- Bezada, M.J., Levander, A., Schmandt, B., 2010. Subduction in the southern Caribbean: images from finite-frequency P wave tomography. *J. Geophys. Res., Solid Earth* 115 (B12).
- Bezada, M.J., Humphreys, E.D., Toomey, D.R., Harnafi, M., Dávila, J.M., Gallart, J., 2013. Evidence for slab rollback in westernmost Mediterranean from improved upper mantle imaging. *Earth Planet. Sci. Lett.* 368, 51–60. <https://doi.org/10.1016/j.epsl.2013.02.024>.
- Billen, M.I., 2020. Deep slab seismicity limited by rate of deformation in the transition zone. *Sci. Adv.* 6 (22), eaaz7692. <https://doi.org/10.1126/sciadv.aaz7692>.
- Bodmer, M., Toomey, D.R., Hoft, E.E.E., Schmandt, B., 2018. Buoyant asthenosphere beneath Cascadia influences megathrust segmentation. *Geophys. Res. Lett.* 45 (14), 6954–6962. <https://doi.org/10.1029/2018GL078700>.
- Borrero, C., et al., 2009. Geochemistry and tectonic controls of the effusive activity related with the ancestral Nevado del Ruiz volcano, Colombia. *Geofis. Int.* 48 (1), 149–169.
- Boschman, L.M., van Hinsbergen, D.J.J., Torsvik, T.H., Spakman, W., Pindell, J.L., 2014. Kinematic reconstruction of the Caribbean region since the Early Jurassic. *Earth-Sci. Rev.* 138, 102–136. <https://doi.org/10.1016/j.earscirev.2014.08.007>.
- Burke, K., 1988. Tectonic evolution of the Caribbean. *Annu. Rev. Earth Planet. Sci.* 16, 201–230 (A88-52285 22-46). Annual Reviews, Inc., Palo Alto, CA.
- Chiarabba, Claudio, et al., 2016. Subduction system and flat slab beneath the Eastern Cordillera of Colombia. *Geochem. Geophys. Geosyst.* 17 (1), 16–27. <https://doi.org/10.1002/2015GC006048>.
- Corredor, Freddy, 2003. Seismic strain rates and distributed continental deformation in the northern Andes and three-dimensional seismotectonics of northwestern South America. *Tectonophysics* 372.3–4, 147–166.
- Cornthwaite, J., Bezada, M.J., Miao, W., Schmitz, M., Prieto, G.A., Dionicio, V., et al., 2021. Caribbean slab segmentation beneath northwest South America revealed by 3-D finite frequency teleseismic P-wave tomography. *Geochem. Geophys. Geosyst.* 22 (4), e2020GC009431. <https://doi.org/10.1029/2020GC009431>.
- Cortés, Martín, Angelier, Jacques, 2005. Current states of stress in the northern Andes as indicated by focal mechanisms of earthquakes. *Tectonophysics* 403 (1–4), 29–58.
- Dahlen, F.A., Hung, S.H., Nolet, G., 2000. Frechet kernels for finite-frequency traveltimes: I, Theory. *Geophys. J. Int.* 141, 157–174.
- Davies, J.H., von Blanckenburg, F., 1995. Slab breakoff: a model of lithosphere detachment and its test in the magmatism and deformation of collisional orogens. *Earth Planet. Sci. Lett.* 129 (1–4), 85–102.
- DeMets, C., Jansma, P.E., Mattioli, G.S., Dixon, T.H., Farina, F., Bilham, R., Calais, E., Mann, P., 2000. GPS geodetic constraints on Caribbean North America plate motion. *Geophys. Res. Lett.* 27, 437–440.
- DeMets, C., 2001. A new estimate for present-day Cocos-Caribbean plate motion: implications for slip along the Central American volcanic arc. *Geophys. Res. Lett.* 28, 4043–4046.
- Garzanti, E., Radeff, G., Malusà, M.G., 2018. Slab breakoff: a critical appraisal of a geological theory as applied in space and time. *Earth-Sci. Rev.* 177, 303–319. <https://doi.org/10.1016/j.earscirev.2017.11.012>.
- Hammond, W.C., Toomey, D.R., 2003. Seismic velocity anisotropy and heterogeneity beneath the Mantle Electromagnetic and Tomography Experiment (MELT) region of the East Pacific Rise from analysis of P and S body waves. *J. Geophys. Res., Solid Earth* 108.
- Kellogg, James N., Bonini, William E., 1982. Subduction of the Caribbean plate and basement uplifts in the overriding South American plate. *Tectonics* 1 (3), 251–276.
- Kellogg, J.N., Vega, V., 1995. Tectonic development of Panama, Costa Rica, and the Colombian Andes: constraints from global positioning system geodetic studies and gravity. In: Mann, P. (Ed.), *Geologic and Tectonic Development of the Caribbean Plate Boundary in Southern Central America*. Geol. Soc. of Am., Boulder, CO, pp. 75–90.
- Kellogg, J., Mora-Páez, H., 2016. Panama Arc-North Andes Collision: “Broken Indenter” model from new GPS velocity field. In: IASPEI—Regional Assembly. Latin American and Caribbean Seismological Commission—LACSC. San José.
- Kellogg, J.N., Camelio, G.B.F., Mora-Páez, H., 2019. Cenozoic tectonic evolution of the North Andes with constraints from volcanic ages, seismic reflection, and satellite geodesy. In: *Andean Tectonics*.
- Kennett, Brian L.N., Engdahl, E.R., Buland, R., 1995. Constraints on seismic velocities in the Earth from traveltimes. *Geophys. J. Int.* 122 (1), 108–124.
- Larmat, C., Maceira, M., Higdon, D.M., Anderson, D.N., 2017. Joining statistics and geophysics for assessment and uncertainty quantification of three-dimensional seismic Earth models. *Stat. Anal. Data Min.* 10 (5), 277–289. <https://doi.org/10.1002/sam.11353>.
- Lonsdale, Peter, 2005. Creation of the Cocos and Nazca plates by fission of the Farallon plate. *Tectonophysics* 404 (3–4), 237–264.
- Ma, Y., Clayton, R.W., 2015. Flat slab deformation caused by interplate suction force. *Geophys. Res. Lett.* 42 (17), 7064–7072. <https://doi.org/10.1002/2015GL065195>.
- Malavé, Gustavo, Suárez, Gerardo, 1995. Intermediate-depth seismicity in northern Colombia and western Venezuela and its relationship to Caribbean plate subduction. *Tectonics* 14 (3), 617–628.
- Masy, J., Niu, F., Levander, A., Schmitz, M., 2011. Mantle flow beneath northwestern Venezuela: seismic evidence for a deep origin of the Mérida Andes. *Earth Planet. Sci. Lett.* 305 (3–4), 396–404. <https://doi.org/10.1016/j.epsl.2011.03.024>.
- McCrorry, P.A., Blair, J.L., Waldhauser, F., Oppenheimer, D.H., 2012. Juan de Fuca slab geometry and its relation to Wadati-Benioff zone seismicity. *J. Geophys. Res., Solid Earth* 117 (B9), B09306. <https://doi.org/10.1029/2012JB009407>.
- Montes, C., Bayona, G., Cardona, A., Buchs, D.M., Silva, C.A., Morón, S., Hoyos, N., Ramírez, D.A., Jaramillo, C.A., Valencia, V., 2012. Arc-continent collision and orocline formation: closing of the Central American seaway. *J. Geophys. Res.* 117, B04105. <https://doi.org/10.1029/2011JB008959>.
- Montes, C., Rodríguez-Corcho, A.F., Bayona, G., Hoyos, N., Zapata, S., Cardona, A., 2019. Continental margin response to multiple arc-continent collisions: the northern Andes-Caribbean margin. *Earth-Sci. Rev.* 198, 102903. <https://doi.org/10.1016/j.earscirev.2019.102903>.
- Mora, J.A., Oncken, O., Le Breton, E., Ibáñez-Mejía, M., Faccenna, C., Vellozo, G., Mesa, A., 2017. Linking Late Cretaceous to Eocene tectonostratigraphy of the San Jacinto Fold Belt of NW Colombia with Caribbean Plateau collision and flat subduction. *Tectonics* 36 (11), 2599–2629. <https://doi.org/10.1002/2017TC004612>.
- Mora-Paez, H., Kellogg, J., Freymueller, J., Mencin, D., Fernandes, R.M., Diederix, H., LaFemina, P., Cardona-Piedrahita, L., Lizarazo, S., Pelaez-Gaviria, J.R., Díaz-Mila, F., Bohorquez-Orozco, O.P., Giraldo-Londoño, L., Corchuelo-Cuervo, Y., 2019. Crustal deformation in the northern Andes – space geodesy velocity field. *J. South Am. Earth Sci.* 89, 76–91. <https://doi.org/10.1016/j.jsames.2018.11.002>.
- Müller, R.D., Sdrolias, M., Gaina, C., Roest, W.R., 2008. Age, spreading rates, and spreading asymmetry of the world’s ocean crust. *Geochem. Geophys. Geosyst.* 9 (4). <https://doi.org/10.1029/2007GC001743>.
- Ojeda, Havskov, 2001. Crustal structure and local seismicity in Colombia. *J. Seismol.* 5 (4), 575–593. <https://doi.org/10.1023/A:1012053206408>.
- Paige, Christopher C., Saunders, Michael A., 1982. LSQR: an algorithm for sparse linear equations and sparse least squares. *ACM Trans. Math. Softw.* 8 (1), 43–71.
- Pennington, W.D., 1981. Subduction of the eastern Panama Basin and seismotectonics of northwestern South America. *J. Geophys. Res.* 86 (B11), 10753–10770.
- Poli, P., Prieto, G.A., Yu, C.Q., Florez, M., Agurto-Detzel, H., Mikesell, T.D., et al., 2016. Complex rupture of the M6.3 2015 March 10 Bucaramanga earthquake: evidence of strong weakening process. *Geophys. J. Int.* 205 (2), 988–994. <https://doi.org/10.1093/gji/ggw065>.
- Porritt, Robert W., Becker, Thorsten W., Monsalve, Gaspar, 2014. Seismic anisotropy and slab dynamics from SKS splitting recorded in Colombia. *Geophys. Res. Lett.* 41 (24), 8775–8783.
- Poveda, E., Julià, J., Schimmel, M., Perez-Garcia, N., 2018. Upper and middle crustal velocity structure of the Colombian Andes from ambient noise tomography: investigating subduction-related magmatism in the overriding plate. *J. Geophys. Res., Solid Earth* 123 (2), 1459–1485. <https://doi.org/10.1002/2017JB014688>.
- Prieto, G.A., Beroza, G.C., Barrett, S.A., López, G.A., Florez, M., 2012. Earthquake nests as natural laboratories for the study of intermediate-depth earthquake mechanics. *Tectonophysics* 570–571, 42–56. <https://doi.org/10.1016/j.tecto.2012.07.019>.
- Rawlinson, N., Spakman, W., 2016. On the use of sensitivity tests in seismic tomography. *Geophys. J. Int.* 205 (2), 1221–1243. <https://doi.org/10.1093/gji/ggw084>.
- Schmandt, Brandon, Humphreys, Eugene, 2010. Complex subduction and small-scale convection revealed by body-wave tomography of the western United States upper mantle. *Earth Planet. Sci. Lett.* 297 (3–4), 435–445. <https://doi.org/10.1016/j.epsl.2010.06.047>.
- Schmandt, B., Humphreys, E., 2011. Seismically imaged relict slab from the 55 Ma Siletzia accretion to the northwest United States. *Geology* 39 (2), 175–178. <https://doi.org/10.1130/G31558.1>.
- Scire, A., Zandt, G., Beck, S., Long, M., Wagner, L., Minaya, E., Tavera, H., 2016. Imaging the transition from flat to normal subduction: variations in the structure of the Nazca slab and upper mantle under southern Peru and northwestern Bolivia. *Geophys. J. Int.* 204 (1), 457–479. <https://doi.org/10.1093/gji/ggv452>.
- Stock, J.M., Lee, J., 1994. Do microplates in subduction zones leave a geological record? *Tectonics* 13 (6), 1472–1487. <https://doi.org/10.1029/94TC01808>.

- Syracuse, Ellen M., et al., 2016. Multiple plates subducting beneath Colombia, as illuminated by seismicity and velocity from the joint inversion of seismic and gravity data. *Earth Planet. Sci. Lett.* 444, 139–149.
- Taboada, Alfredo, et al., 2000. Geodynamics of the northern Andes: subductions and intracontinental deformation (Colombia). *Tectonics* 19 (5), 787–813. <https://doi.org/10.1029/2000TC900004>.
- Toomey, D., Solomon, S., Purdy, G., 1994. Tomographic imaging of the shallow crustal structure of the East Pacific rise at 9-degrees-30'n. *J. Geophys. Res., Solid Earth* 99, 24135–24157.
- Trenkamp, R., Kellogg, J.N., Freymueller, J.T., Mora, H.P., 2002. Wide plate margin deformation, southern Central America and northwestern South America, CASA GPS observations. *J. South Am. Earth Sci.* 15 (2), 157–171.
- van Benthem, S., Govers, R., Spakman, W., Wortel, R., 2013. Tectonic evolution and mantle structure of the Caribbean. *J. Geophys. Res., Solid Earth*. <https://doi.org/10.1002/jgrb.50235>.
- VanDecar, J.C., Crosson, R.S., 1990. Determination of teleseismic relative phase arrival times using multi-channel cross-correlation and least squares. *Bull. Seismol. Soc. Am.* 80 (1), 150–169.
- van der Hilst, Rob, Mann, Paul, 1994. Tectonic implications of tomographic images of subducted lithosphere beneath northwestern South America. *Geology* 22 (5), 451–454.
- Vargas, Carlos A., Mann, Paul, 2013. Tearing and breaking off of subducted slabs as the result of collision of the Panama Arc-indenter with northwestern South America. *Bull. Seismol. Soc. Am.* 103 (3), 2025–2046.
- Wagner, L.S., et al., 2017. Transient slab flattening beneath Colombia. *Geophys. Res. Lett.* 44 (13), 6616–6623.
- Weber, J.C., Dixon, T.H., DeMets, C., Ambeh, W.B., Jansma, P., Mattioli, G., Saleh, J., Sella, G., Bilham, R., Perez, O., 2001. GPS estimate of relative motion between the Caribbean and South American plates, and geologic implications for Trinidad and Venezuela. *Geology* 29 (1), 75–78.
- Zarifi, Z., Havskov, J., Hanyga, A., 2007. An insight into the Bucaramanga nest. *Tectonophysics* 443 (1–2), 93–105.
- Zhang, T., Gordon, R.G., Mishra, J.K., Wang, C., 2017. The Malpelo Plate Hypothesis and implications for nonclosure of the Cocos-Nazca-Pacific plate motion circuit. *Geophys. Res. Lett.* 44 (16), 8213–8218. <https://doi.org/10.1002/2017GL073704>.